Title

Computational analysis of the environment in an indoor vertical farming system

Authors

Naranjani, B
Najafianashrafi, Z
Pascual, C
et al.

Publication Date

2022-05-01

DOI

10.1016/j.ijheatmasstransfer.2021.122460

Peer reviewed

International Journal of Heat and Mass Transfer 186 (2022) 122460

Contents lists available at ScienceDirect

International Journal of Heat and Mass Transfer

journal homepage: www.elsevier.com/locate/hmt

Computational analysis of the environment in an indoor vertical farming system

Benyamin Naranjani[a], Zabihollah Najafianashrafi[a], Christopher Pascual[b], Ireneo Agulto[b], Po-Ya Abel Chuang[a,*]

[a] Department of Mechanical Engineering, University of California, Merced, 5200 North Lake Road, Merced, CA 95343, USA
[b] Department of Agricultural and Biosystems Engineering, Central Luzon State University, Science City of Munoz 3120, Nueva Ecija, Philippines

ARTICLE INFO

Article history:
Received 10 August 2021
Revised 15 December 2021
Accepted 19 December 2021

Keywords:
Computational fluid dynamics
Turbulent flow
Uniformity
Indoor vertical farming system
Photosynthesis modeling
Lettuce

ABSTRACT

The increasing demand for agricultural products and scarcity of resources, such as soil fertility, irrigation water, and moderate climate, have driven increased use of indoor vertical farming systems. In this paper, a three-dimensional numerical model is developed to optimize air flow and heat transfer within an indoor system considering transpiration, carbon-dioxide consumption, and oxygen production. The near-wall RNG $k-\varepsilon$ turbulent model is implemented to consider the impacts of turbulence and obstacles in the computational domain. To assess the degree of uniformity affecting each tray, an objective uniformity parameter is developed based on the deviation of flow velocity over cultivation trays with respect to the optimal flow velocity. Further, an efficiency parameter is defined based on relative humidity, temperature, and pressure drop to holistically compare the effectiveness of flow inlet and outlet locations. Accordingly, eight designs are studied extensively and one case is found to be the most efficient with an objective uniformity of 91.7% due to high degree of spiral flow circulation. Most importantly, the results suggest that some cases even with low mass flow rates are capable of providing uniform flow distribution, which can significantly reduce energy consumption of indoor vertical farming systems. This newly developed model is proven to be an effective tool for investigating the heat transfer rate and fluid flow uniformity and optimizing cultivation environment for an indoor vertical farming system.

1. Introduction

According to the United Nations, the population of the world is expected to grow in the next century, which in turn encourages the development of innovative techniques to ensure agricultural sustainability. Agriculture on productive land is threatened not only by high levels of urbanization [1], uneven water distribution [2], and inclement weather [3], but also is threats to biodiversity that have unfavorable environmental impacts [4,5]. Due to the anticipated drastic population growth and constraints on resources in the upcoming decades, only 10% of the demand for food is estimated to be met by expansion of productive lands, with the remainder relying on new techniques that can achieve higher yields [6]. Therefore, developing novel methods to augment the ratio of crop production over used land is a vital issue [7].

In recent years, the indoor vertical farming systems (IVFS) with artificial light are found to be a viable solution to resolve the increasing demands of future agricultural products [8]. The IVFS are promising alternatives to open field or greenhouse agriculture because they have precisely monitoring environmental parameters and are insensitive to outdoor climates, which can boost annual sales volume per unit area up to 100 times compared to that of open lands [9]. Furthermore, employment of light emitting diodes (LED) as light sources can initiate and sustain photosynthesis reactions and the optical wavelength, light intensity, and radiation intervals can further enhance growth quality [10]. Recently, many studies have been carried out to investigate how environmental parameters, such as closed-loop control [11], ultrasound [12], and electro-degradation [13], affect hydroponic cultivation of leafy vegetables in these systems.

One of the most influential factors affecting growth in IVFS is to maintain a uniform air flow at an optimal air current speed over plants canopy surfaces. Poor flow uniformity or variation in air velocity over culture beds destabilizes crop production rates [14]. It has been found that inducing a horizontal air speed of 0.3–0.5 m s^{-1} boosts photosynthesis through more efficiently exchanging species between the stomatal cavities in plants and the

* Corresponding author.
E-mail address: abel.chuang@ucmerced.edu (P.-Y.A. Chuang).

https://doi.org/10.1016/j.ijheatmasstransfer.2021.122460

Nomenclature

A, B, C, D	positions of supplying air inlet/outlet on room wall
C_p	specific heat capacity, J kg^{-1} K^{-1}
g	gravitational acceleration, m s^{-2}
H	room height, m
j	vector variable of turbulent mass diffusion flux, kg m^{-2} s^{-1}
k	turbulent kinetic energy, m^2 s^{-2}
L	room length, m
Nu	Nusselt number
OU	objective uniformity
P	power, W
p	pressure, Pa
Q	volumetric flow rate, m^3 s^{-1}
R	rate of chemical mass production, kg m^{-3} s^{-1}
Re	Reynolds number
RH	relative humidity
S	user-defined source term of mass production, kg m^{-3} s^{-1}
S_T	heat source or sink, W m^{-3}
S_U	standard deviation of velocity, m s^{-1}
T	temperature, K
t	thickness of room wall, m
t	time, s
u	velocity vector component, m s^{-1}
U	average free stream velocity above the tray, m s^{-1}
U_0	desired air speed above the tray, m s^{-1}
W	room width, m
x	cartesian coordinates, m

Greek symbols

γ	specie mass fraction
δ	kronecker delta
ε	dissipation rate of turbulent kinetic energy, m^2 s^{-3}
η	efficiency factor
λ	thermal conductivity, W m^{-1} K^{-1}
μ	dynamic viscosity, kg m^{-1} s^{-1}
ρ	fluid density, kg m^{-3}

Subscripts

i, j	cartesian coordinates index
k	k-th specie
n	n-th tray

flow of air [15]. Lee et al. studied the effects of air temperature and flow rate on the occurrence of lettuce leaf tip burn (a calcium deficiency disorder) in a closed plant factory system [16]. Furthermore, it was observed that the relative humidity of the air flow can significantly influence calcium transportation in lisianthus cultivars [17]. According to Vanhassel et al., higher levels of relative humidity can significantly decrease the occurrence of tip burn [18]. Therefore, it is vital to maintain relative humidity in the desired range to ensure even distribution of calcium in lettuce leaves. Over the past few years, researchers have been trying to develop techniques for improving uniformity over cultivation zones [19,20].

Regardless of the recent progress, the control and automation systems of IVFS bring additional costs, which makes systematic experimental investigation and optimization a challenge. Computational fluid dynamics (CFD) has been utilized as a reliable tool to numerically simulate complex physical phenomena. Markatos et al. developed a CFD procedure to study velocity and temperature distribution in enclosures using buoyancy-induced physics [21]. Stavrakakis et al. investigated the capability of three Reynolds-Averaged Navier-Stokes (RANS) models to simulate natural ventilation in buildings [22]. Papakonstantinou et al. presented a mathematical model for turbulent flow and accordingly developed a 3-D numerical code to compute velocity and temperature fields in buildings [23]. A novel gas-liquid mass transfer CFD model was developed by Li et al. to simulate the absorption of CO_2 in a microporous microchannel reactor [24]. Yuan et al. visualized the air paths and thermal leakages near a complex geometry using a transient thermal model with buoyancy-driven convection, conduction and thermal radiation heat transfer and flow field near a vehicle structure [25]. In the context of agriculture, researchers have extensively employed CFD analysis for study of ventilation, air flow, and microclimate in indoor systems [26–29]. Zhang et al. developed a CFD simulation to assess single-phase turbulent air stream in an indoor plant factory system and achieved the highest level of flow uniformity with two perforated tubes [30]. Karadimou and Markatos developed a transient two-phase model to study particle distribution in the indoor environment using Large Eddy Simulation method [31]. Baek et al. used CFD analysis to study various combinations of air conditioners and fans to improve growth rate in a plant factory [32]. More recently, Niam et al. [33] performed numerical investigation and determined the optimum position of air conditioners in a small vertical plant factory is over the top. In addition, a variety of mathematical techniques are proposed to provide sub-model for investigating photosynthesis [34]. According to Boulard et al., tall canopies can induce a stronger cooling of the interior air by using a CFD model to study the water vapor, temperature, and CO_2 distribution in a Venlo-type semi-closed glass greenhouse [35].

Despite the fact that photosynthesis plays an integral role in distribution of species and uniformity along cultivation trays, this issue has not been well addressed. Although numerous research works have been done to investigate the turbulent flow in enclosures and buildings, this study is the first to numerically investigate the transport phenomena considering the product generation and reactant consumption through photosynthesis and plants transpiration with CFD simulations for IVFS-based studies. Furthermore, a newly proposed objective uniformity parameter is defined to quantify velocity uniformity for individual cultivation trays. Moreover, numerical simulations are performed to simulate and optimize fluid flow and heat transfer in an IVFS for eight distinct placements of flow inlets and outlets in this study. Accordingly, the effects of each case on uniformity, relative humidity, temperature, and carbon dioxide concentration are discussed in detail. Finally, an overall efficiency parameter is defined to provide a holistic comparison of all parameters and their uniformity of each case.

2. Modeling of the problem and boundary conditions

In this study, three-dimensional modeling of conjugated fluid flow and heat transfer is performed to simulate the turbulent flow inside a culture room having four towers for hydroponic lettuce growth. Assuming that the four towers are symmetric, a quarter of the room (one tower) with four cultivation trays is selected as the computational domain, as illustrated in Fig. 1a. Symmetry boundaries are set at the middle of the length and width of the room. The effect of LED lights on heat transfer is considered through constant heat flux boundary conditions at the bottom surface of each tray as shown in Fig. 1b. Lastly, the species transfer due to photosynthesis are occurring only in the exchange zone, which is illustrated in Fig. 1c. To study the impact of air inlet/exit locations on characteristics of air flow, four square areas, denoted as A, B, C, and D in Fig. 1a, are considered to be inlet, exit, or wall. To perform a systematic study, Table 1 presents the location of inlet and exit for all eight cases studied. With the aim of comparing all of the proposed designs, case AB is selected to be the baseline.

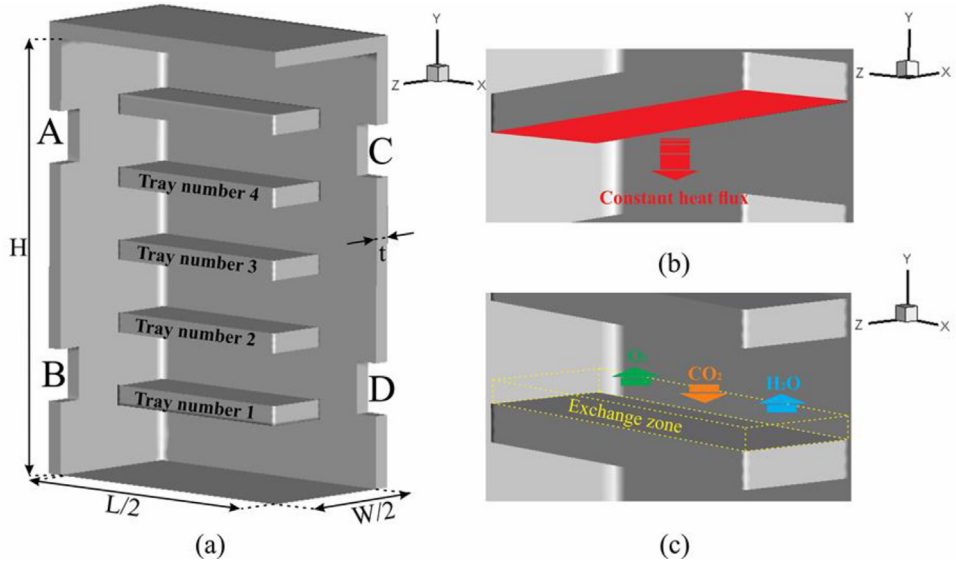

Fig. 1. (a) Schematic of the computational domain, (b) illustration of constant heat flux at the bottom of each tray, and (c) illustration of the exchange zone above each tray with indications of species transfer.

Table 1
Placement of the inlet and outlet for eight studied cases.

Boundaries	A	B	C	D
Case AB, Baseline	Mass flow inlet	Pressure outlet	Wall	Wall
Case AD	Mass flow inlet	Wall	Wall	Pressure outlet
Case BA	Pressure outlet	Mass flow inlet	Wall	Wall
Case BC	Wall	Mass flow inlet	Pressure outlet	Wall
Case CB	Wall	Pressure outlet	Mass flow inlet	Wall
Case CD	Wall	Wall	Mass flow inlet	Pressure outlet
Case DA	Pressure outlet	Wall	Wall	Mass flow inlet
Case DC	Wall	Wall	Pressure outlet	Mass flow inlet

Table 2
Dimensions and boundary conditions.

Domain	Dimensions: Length(L) × Width(W) × Height(H)
Room	4.4 × 2.2 × 3.3 m^3
Lettuce trays	1.6 × 0.5 × 0.15 m^3
Photosynthesis exchange zone	1.6 × 0.5 × 0.1 m^3
Wall thickness(t)	0.12 m
Boundary conditions	Specifications
Inlet: Mass flow inlet	0.1∼0.5 kg s^{-1}, 291.15 K
Outlet: Pressure outlet	Zero pressure
LED: Constant heat flux	500 W m^{-2} (LED Grow Lights Depot, 2018)
Outside wall: constant temperature	301.15 K

To consider the effect of heat transfer with the outdoor ambient air, a solid wall zone comprised of plywood with a thickness of 0.12 m is assumed in the simulation. A constant-temperature boundary condition is set on the outer surface of the wall. Both conduction and convective heat transfer are considered within the model. All dimensions and boundary conditions are listed in Table 2.

In our model, the species exchange zone of photosynthesis is defined to be directly above the upper surface of each tray. These zones have the same cross-sectional area as the trays with the height of 0.1 m. Within the exchange zone, the water transpiration rate and carbon dioxide consumption rate are defined according to the experimental data obtained by Jin et al. [36] and Adeyemi et al. [37]. Then, the CO_2 consumption rate and O_2 production rate are calculated and set based on the molar balance of the photosynthesis reaction equation as the following:

$$6CO_2(\text{gas}) + 6H_2O(\text{liquid}) + \textit{Light Energy} \rightarrow C_6H_{12}O_6(\text{solid}) + 6O_2(\text{gas}) \quad (1)$$

Notably, the liquid water on the left-hand side of Eq. (1) is assumed to be provided through hydroponic water circulation of an IVFS. Nevertheless, liquid water consumption and solid sugar production are not modeled in this computational study. Also, the required light energy for photosynthesis is provided through the LED lights. The overarching goal of this work is to enhance indoor air and relative humidity distribution for optimizing photosynthesis processes.

Based on the assumed 0.15 m plant density, each cultivation tray houses a total number of 44 lettuces. Moreover, each lettuce is considered to have an average leaf area of 0.015 m^2. Accordingly,

Table 3
Materials and properties.

Characteristics of flow at inlet	
Fluid flow	Mixture of CO_2, O_2, H_2O, and N_2
CO_2 mass fraction	0.153%
O_2 mass fraction	23.24%
Relative humidity	85%
Mixture density	Incompressible ideal gas
Mixture specific heat	Mixing law
Mixture viscosity	1.72×10^{-5} kg m^{-1} s^{-1}
Exchange zone	
CO_2 consumption rate	3.160×10^{-5} kg m^{-3} s^{-1}
O_2 production rate	2.297×10^{-5} kg m^{-3} s^{-1}
H_2O transpiration rate	2.489×10^{-4} kg m^{-3} s^{-1}
Wall zone	
Wood density	700 kg m^{-3}
Wood specific heat	2310 J kg^{-1} K^{-1}
Wood thermal conductivity	0.173 W m^{-1} K^{-1}

the production and consumption rates of gaseous species of the photosynthesis reaction are estimated based on the empirical data [36,37]. Specific input values of the inlet flow, photosynthesis rate, and wall properties are reported in Table 3.

3. Numerical procedure and data analysis

3.1. Mathematical modeling and governing equations

The main objective of this work is to study the flow pattern, uniformity and heat transfer inside the IVFS numerically. The flow is assumed to be steady-state, three-dimensional, incompressible, and Newtonian. Due to the high inertia of the inlet flow and the presence of the lettuce trays as obstacles, the flow is assumed to be fully turbulent throughout the room. In the past few years, the $k-\varepsilon$ model has been widely used for turbulent flow simulation in agricultural applications [38–40]. Therefore, the Re-Normalization Group (RNG) $k-\varepsilon$ turbulence model is applied to our model. The time-averaged governing equations of continuity, momentum and energy can be derived in three-dimensional Cartesian coordinate system as the following:

$$\frac{\partial}{\partial x_j}\left(\rho u_j\right) = 0 \tag{2}$$

$$\frac{\partial}{\partial x_j}\left(\rho u_i u_j\right) = \frac{\partial}{\partial x_j}\left[-P\delta_{ij} + \mu\left(\frac{\partial u_i}{\partial x_j} + \frac{\partial u_j}{\partial x_i}\right)\right] + \rho g_i \tag{3}$$

$$\frac{\partial}{\partial x_j}\left(\rho u_j C_p T\right) - \frac{\partial}{\partial x_j}\left(\lambda\frac{\partial T}{\partial x_j}\right) = S_T \tag{4}$$

where the index notations $i, j = 1, 2, 3$, the variable x_j is the direction in three dimensional Cartesian coordinate system, and parameters ρ, u_j, δ_{ij}, μ, and T stand for density, time-averaged velocity, Kronecker delta, effective dynamic viscosity incorporating turbulence effects, and time-averaged temperature, respectively. The last term on the right-hand side of Eq. (3) represents the effect of buoyancy forces in momentum equation. Additionally, C_p denotes specific heat capacity, λ represents thermal conductivity and S_T is the heat sink or source. In the present work, the value of S_T is zero throughout the computational domain since there is no additional volumetric heat source or sink other than the LED lights, which is considered surface heat source input implemented boundary conditions.

To incorporate turbulence in the simulation, the RNG $k-\varepsilon$ model solves two additional transport equations for the kinetic energy, k, and the attributed dissipation rate, ε. The model utilizes an analytical differential relation to determine the effective viscosity, which is then applied to μ in the momentum equation. The RNG $k-\varepsilon$ turbulence model has one additional term in the transport equation for enhanced solution of the rapid strains and swirls, which applies in the IVFS due to tray and crop blockage.

The fluid flow inside the culture room is assumed to be a mixture of water vapor, oxygen, carbon dioxide, and nitrogen. In the exchange zone defined in Fig. 1c, the influence of photosynthesis on species concentration is included in the simulation through either sources or sinks. Thereafter, for each of the reaction species, a convection-diffusion transport equation is solved to obtain the related local mass fraction. The species mass fraction transport equation can be written as:

$$\frac{\partial}{\partial x_j}\left(\rho u_j \gamma_n\right) = -\frac{\partial j_{n,j}}{\partial x_j} + R_n + S_n \tag{5}$$

where the subscript "n" refers to the characteristics of nth specie, γ is the species mass fraction, j_j denotes the vector variable of turbulent mass diffusion flux caused by the gradients of temperature and concentration, and R and S represent the rate of chemical production and user-defined source terms, respectively. In our numerical model, the value of R is set to be zero since there is no chemical reactions involved. Similarly, the value of S is set to be zero, except in the exchange zones, where the species production and consumption rates as shown in Table 3 are taken into consideration. Since there are four species involved in the system, only three transport equations as shown in Eq. (5) need to be solved and the last specie can be obtained by subtracting the sum of all other species from unity. To enhance the numerical precision, nitrogen is selected to be the last specie due to its maximum mass fraction among all other ones.

To solve all aforementioned flow equations, a commercially available software on the basis of finite-volume approach is used. In order to efficiently treat the pressure-velocity coupling phenomena, SIMPLEC algorithm [41] is employed to solve the Navier-Stokes flow equations. In terms of spatial discretization, the least square cell-based method is considered for gradient terms and the second-order accuracy upwind scheme is used to discretize the convective and diffusive terms. Lastly, parallel computations are carried out on 4 cores of an Intel Core-i7–3520 m processor (2.90 GHz) for this study.

4. Data analysis and uniformity assessment

Previous research has shown that horizontal air flow through the crops can enhance carbon dioxide diffusion which, in turn, boosts photosynthesis and growth rates [42]. The IVFS with the aid of controlled air flow and ventilation are capable of enhancing this diffusion effect to maximize cultivation efficiency. Nevertheless, the variation of air velocity over different trays leads to non-uniformity of carbon dioxide distribution. To minimize this adverse effect, achieving more uniform flow for each tray is important for every IVFS design. In this study, we define parameters to assess flow uniformity, power required, and overall design efficiency. The standard deviation of the flow distribution inside the room with respect to a target speed can be calculated as:

$$S_U = \sqrt{\frac{1}{N-1}\sum_{k=1}^{N}\left(U_k - U_o\right)^2} \tag{6}$$

where U_k is the average velocity over the upper surface of the k-th tray exchange zone, U_o is the desired air speed, and N is the number of trays inside the system. In this study, U_o is selected to be 0.4 m s^{-1}, a value shown previously to enhance photosynthesis for lettuce cultivation [15]. A dimensionless objective uniformity parameter, OU, is defined as the variation of the velocity distribution for all cultivations zones and can be written as:

$$OU = \left(1 - \frac{S_U}{2U_o}\right) \tag{7}$$

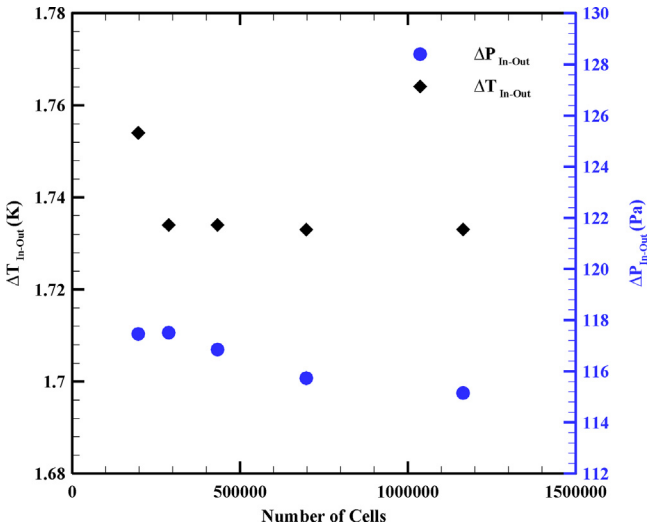

Fig. 2. Results of grid sensitivity study for the baseline case AB at a mass flow rate of 1 kg s^{-1}.

The required power of the fans for circulation of flow throughout the room is calculated by:

$$P = Q\Delta p \tag{8}$$

where $P$is the required power to drive the flow, Q is the volumetric flow rate and Δp is the pressure increase across the fans. To assess the combined effects of velocity distribution, species and temperature uniformity, and required power, an efficiency factor, η, is defined as:

$$\eta = \frac{OU\,\frac{\overline{RH}}{\overline{RH}_{\text{Inlet}}}\,\frac{\overline{CO_2\,ppm}}{\overline{CO_2\,ppm}_{\text{Inlet}}}}{\frac{P}{P_{\text{Baseline}}}\,\frac{\overline{T}}{\overline{T}_{\text{Inlet}}}} \tag{9}$$

where the bar denotes the average value obtained from the top surfaces of all the exchange zones.

5. Grid study and validation

In our model, a tetrahedral grid type is used to discretize the entire computational domain. To ensure that the numerical results are independent of grid dimensions, five grid numbers ranging from 196,951 (coarse) to 1,164,624 (fine) are used to study the baseline Case AB at a mass flow rate of 1 kg s^{-1}. Fig. 2 summarizes the average temperature and pressure difference (between the inlet and outlet) for the five grid numbers. Balancing between the accuracy of the simulation results and computational cost, the grid number of 697,537 is employed throughout the rest of the study.

The simulation domain consists of rectangular prisms as cultivation tray, the exchange zone in which the photosynthesis processes occur, and the rest of the open volume. To validate our numerical code, we performed simulation of conjugated heat transfer and turbulent flow passing over one rectangular prism in a duct. The exact dimensions and input conditions of this test case can be found in the study of Nakagawa et al. [43]. The induced flow involves periodic vortex shedding that can be problematic for numerical analysis. The results of the numerical simulations are compared with the experimental measurements done by Lyn et al. [44], Franke and Rodi [45], and Durao et al. [46]. Fig. 3 shows the average axial velocity distribution and our simulation results agree well with the experimental data both before and after the rectangular prisms. To further validate the reliability of heat transfer calculation, the simulated local Nusselt number along the upper wall of the square prism are compared with the experimental data measured by Nakagawa et al. [43] in Fig. 4. When x/H is between 1 and 2, the wake flow is extremely unsteady and adverse flow can be observed in Fig. 3. Therefore, it is extremely difficult to accurately predict the convective heat transfer in this region. Nevertheless, the simulation results show good agreement with the experimental data, especially in the wake region (x/H > 2). Further, the calculation of species transport in this work is simulated using species exchange sub-model, which has been validated extensively in the literature [39,47–49].

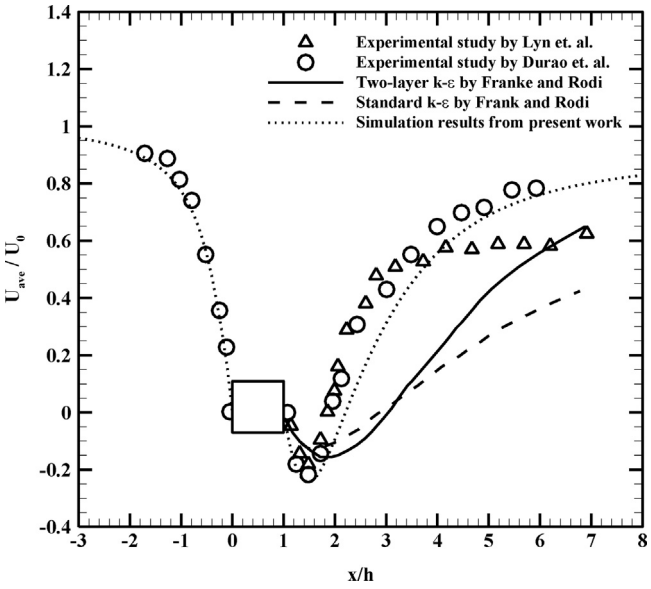

Fig. 3. Normalized average velocity in x direction along the centerline passing through the centroid of the square prism.

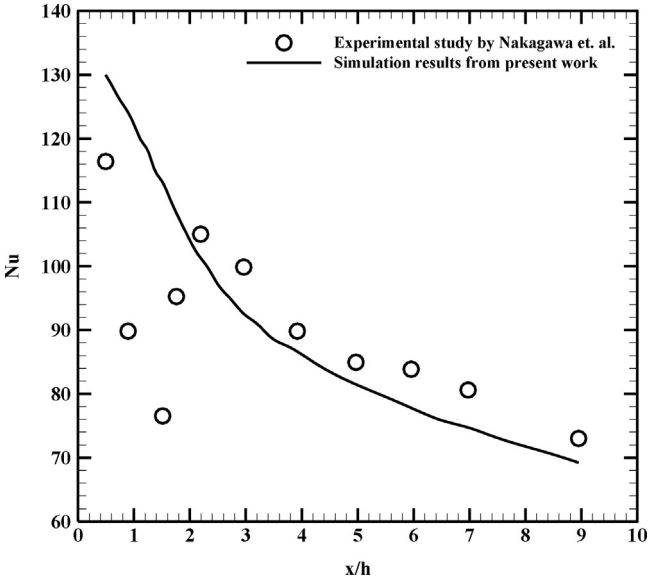

Fig. 4. Local Nusselt number along the centerline passing through the upper confining wall of the square prism for Re = 22,500.

6. Results and discussions

In this study, three dimensional simulations of conjugated turbulent flow and heat transfer are carried out to study the concept of the IVFS. The exchange zone above each tray is designed to represent the volume where the photosynthesis reaction takes place including carbon dioxide consumption along with water transpiration and oxygen production. In addition, the room is assumed to

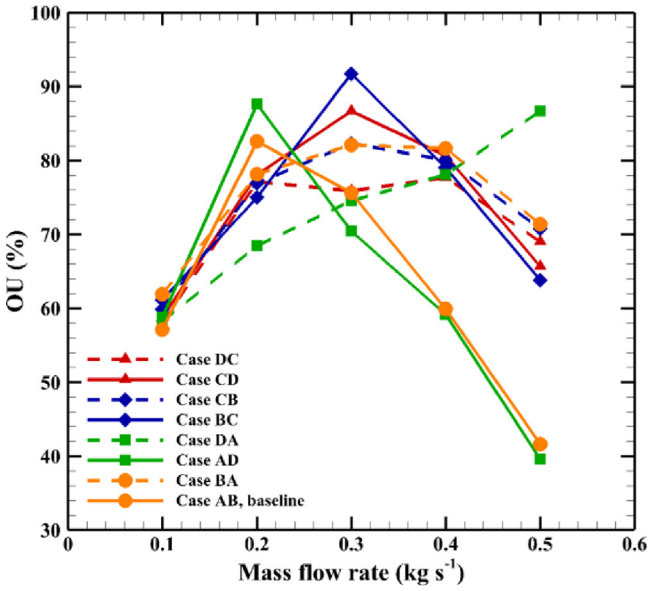

Fig. 5. The objective uniformity (*OU*) as a function of mass flow rate for all eight inlet-outlet placement cases.

be insulated by wooden walls with known thickness and thermal properties for modeling heat exchange with the outdoor ambient air. In this study, we analyze the effect of eight distinctive inlet-outlet placements on flow uniformity over the lettuce canopy, temperature and relative humidity distribution in the room, and the power required for air circulation.

6.1. Objective uniformity (OU)

One of the most critical factors affecting crop growth rate is the air flow velocity over plants. A fluid stream with horizontal speed ranging from 0.3 to 0.5 m s^{-1} can escalate the species exchange between the flow and plant leaves resulting in enhancement of photosynthesis [15]. In indoor farming systems, the flow velocity can be controlled well using ventilation fans for more efficient plant growth. However, heterogeneous distribution of feeding air over plant trays can cause undesirable non-uniformity in crop production, which should be avoided. Therefore, it is important to study the effect of inlet-outlet location and flow rate on the flow patterns throughout the culture room. Herein, the most favorable condition is defined as the condition at which the flow velocity above all trays is equal to the optimum speed U_o, which is set to be 0.4 m s^{-1}. The objective uniformity, *OU*, defined in Eq. (7) is used to assess the overall flow conditions. The *OU* for all eight cases as a function of mass flow rate are summarized in Fig. 5.

Since the inlet/exit area and air density remain the same, the mass flow rate is directly proportional to flow velocity. In addition, the target flow velocity over the plants is set to be 0.4 m s^{-1}. Therefore, a general trend of *OU* first increases and then decreases when increasing the overall mass flow rate. Depending on the design, the peak of *OU* occurs at different mass flow rate for each case. Another general trend can be observed that the peak of *OU* occurs at a lower mass flow rate if the inlet is located at the top due to buoyancy force. This can be clearly demonstrated by cases AB (0.2 kg s^{-1}) and BA (0.3 kg s^{-1}) or AD (0.2 kg s^{-1}) and DA (0.5 kg s^{-1}). Therefore, there exists a different optimal inlet/exit design for each mass flow rate condition. As can be seen from Fig. 5, the maximum *OU* at flow rates of 0.2, 0.3, 0.4 and 0.5 kg s^{-1} is observed for configurations AD, BC, BA, and DA, respectively. Therefore, this simulation model can identify optimal flow configuration at a specific mass flow rate condition.

Since *OU* quantifies the deviation of average velocity of each tray from the designed velocity, a higher *OU* value indicates that the crops will have better and more uniform photosynthesis. It can be observed from Fig. 5 that the maximum *OU* obtained for all conditions is case BC at a flow rate of 0.3 kg s^{-1}. To develop a better understanding, the two-dimensional velocity and vorticity distributions in the x-y plane along the middle of the z-direction for all eight cases at a mass flow rate of 0.3 kg s^{-1} are plotted in Figs. 6 and 7.

As can be observed from Figs. 6 to 7, the OU is highest for case BC due to its uniform velocity and vorticity distributions between trays. This can be attributed to the position of inlet/exit location with respect to the tray orientation. For case BC, the inlet flow is parallel to the longitudinal direction of the tray (x-axis) and the exit is along the transverse direction (z-direction). This design allows the flow to travel through the long side of the tray uninterrupted and then form a helical flow orientation near the end of the tray. This spiral formation of flow induces a more uniform and regular flow in the room. This also explains why case AD has very high *OU*. Similar spiral formation can also be observed when the inlet flow is parallel to the transverse direction of the tray (z-axis) and the exit is along the longitudinal direction (x-direction), like case DA. However, since the inlet flow is along the short side of the tray, the benefit is not as great and requires much higher inlet mass flow rate. On the other hand, for cases where the inlet and exit are located on the same wall, such as AB or CD, the air flow only has strong mixing effect along the inlet/exit direction which, in turn, reduces the overall flow uniformity.

Besides the velocity distribution, the effect of temperature is also a critical parameter for determining convective flow. Fig. 8 shows the two-dimensional temperature distributions in the x-y plane along the middle of the z-direction for all eight cases at a mass flow rate of 0.3 kg s^{-1}. In our analysis, the temperature of the inlet flow is lower than that of the exit flow due to the heat generated from the LED light. For case BC, the inlet is located near the bottom and the exit is near the top. Due to the density difference, the exit warm stream tends to flow up. This allows the flow to reach the topmost tray more easily and, therefore, achieves more uniform temperature distribution among all trays. Combining the inlet flow along the long side of the tray, the helical flow effect, and the buoyancy, case BC is able to reach the maximum *OU* of 91.7%.

Fig. 9 summarized the velocity and temperature contours for case BC at an inlet mass flow rate of 0.3 kg s^{-1}. The velocity profiles in Fig. 9a clearly show the spiral effect above each cultivation tray and the local velocity is close to the optimal speed of 0.4 m s^{-1}. In addition, the temperature shows an increasing trend from bottom to top as the flow helically passing through the crops and moving towards the outlet.

6.2. Temperature and species distribution in the exchange zone

The distributions of temperature and gas species, such as water vapor and CO_2, play an integral role in photosynthesis which, in turn, influences the quality of plant and its growth. Therefore, maintaining these critical parameters in a reasonable range to ensure reliable and efficient production is essential to environmental control of an IVFS. Evaluating the distribution of these parameters can also provide the effectiveness of inlet/exit location. It should be noted that the parameter *OU* provides an overall assessment of the air flow velocity over planting trays. An optimal design is to achieve desired local temperature and species distribution while maintaining high *OU* values in an IVFS. In the following discussion, the four cases with highest values of *OU* at their corresponding mass flow rates are studied and compared to the baseline case AB.

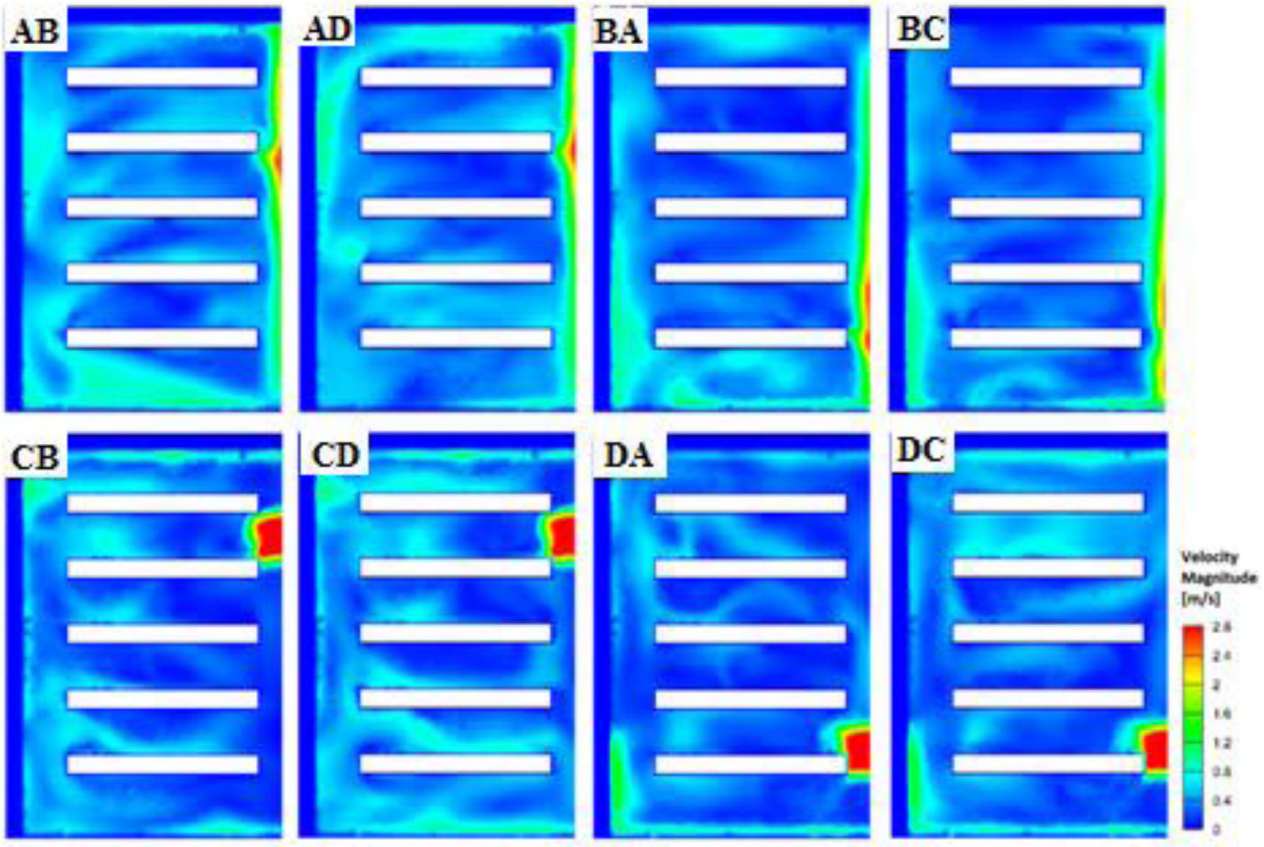

Fig. 6. Two-dimensional velocity distribution of eight inlet-outlet placement cases at a mass flow rate of 0.3 kg s^{-1}.

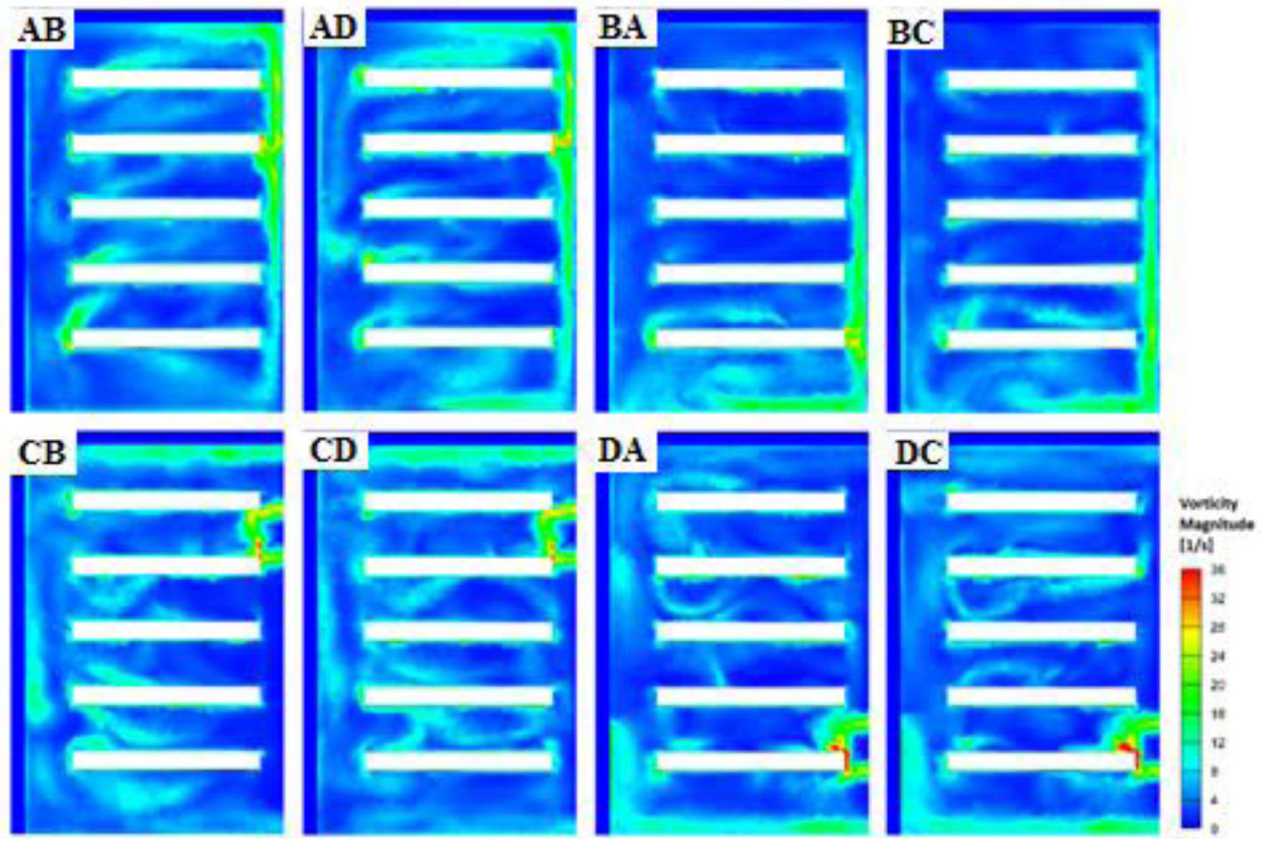

Fig. 7. Two-dimensional vorticity distribution of eight inlet-outlet placement cases at a mass flow rate of 0.3 kg s^{-1}.

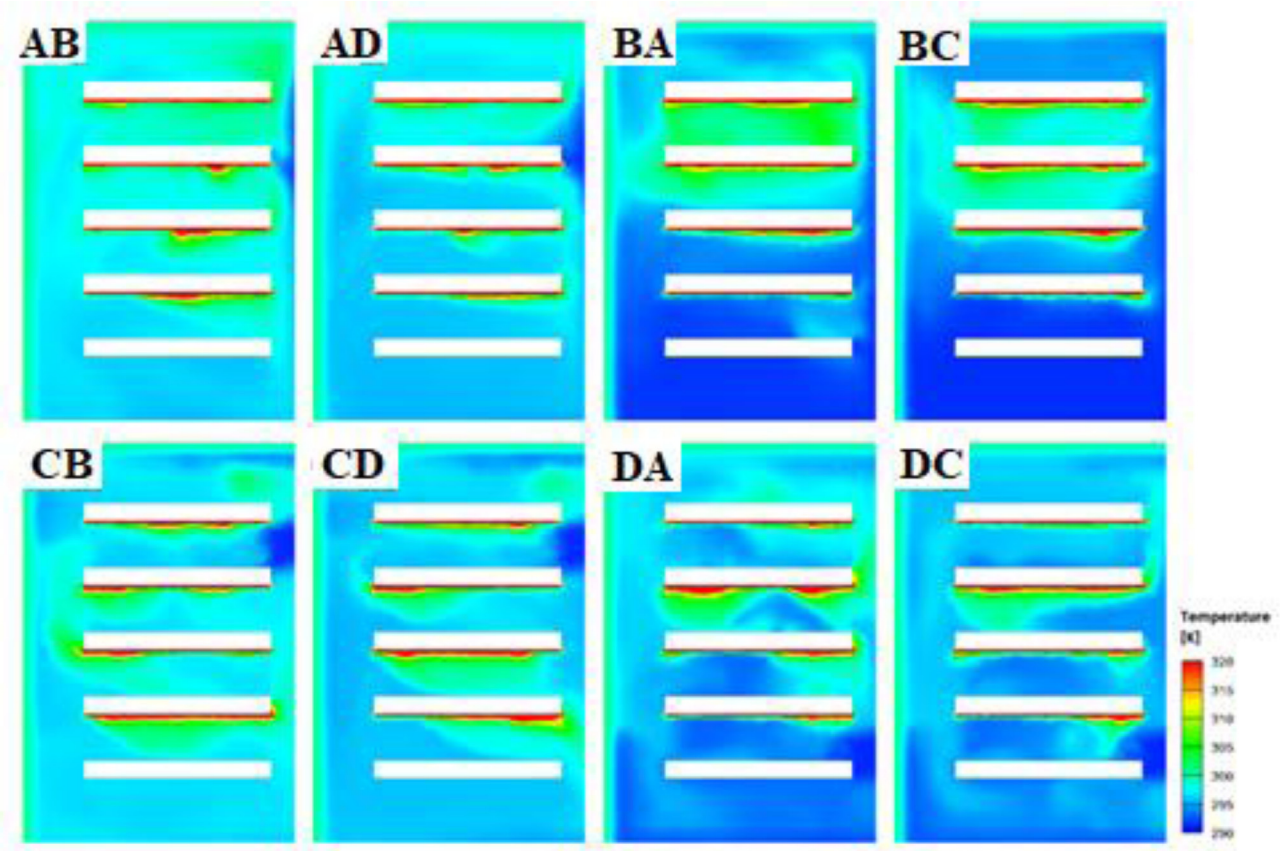

Fig. 8. Two-dimensional temperature distribution of eight inlet-outlet placement cases at a mass flow rate of 0.3 kg s^{-1}.

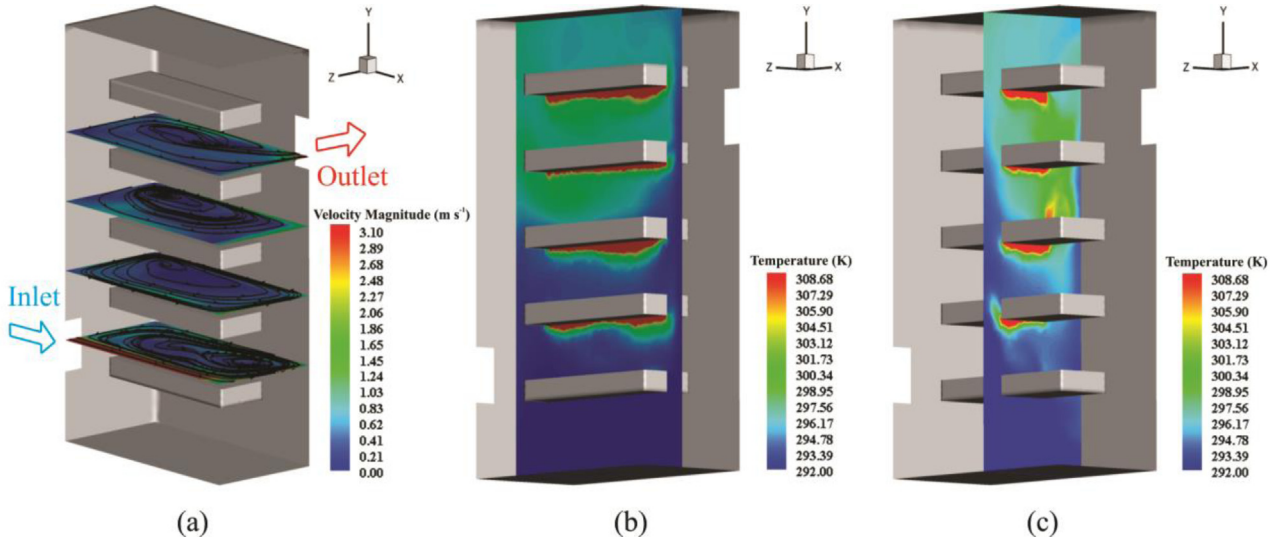

Fig. 9. Local distribution of case BC with the inlet mass flow rate of 0.3 kg s^{-1}: (a) velocity contour along the horizontal plane at the upper surface of the exchange zone of each tray, and temperature contours along the vertical plane at the middle of the tray in the (b) longitudinal direction and (c) transverse direction.

Since CO_2 is a reactant of photosynthesis, increasing CO_2 concentration usually leads to enhancement of crop production. Reports show that increasing the CO_2 concentration from the atmospheric average of 400 ppm to 1500 ppm can increase the yield by as much as 30% [50]. In this IVFS analysis, the CO_2 level of the inlet mass flow rate is increased by a CO_2 generator to be 1000 ppm (= 0.153% mass fraction). Since the consumption rate of CO_2 through the exchange zones is fixed, higher overall average CO_2 concentration through the system is desirable. Fig. 10 shows the comparison of the average CO_2 concentration between the highest *OU* cases and the baseline case AB at different inlet mass flow rate. A few general trends of CO_2 concentration can be observed from Fig. 10. First, the CO_2 concentration increases with inlet flow rate due to increasing supply of CO_2 molecules. In addition, tray 1 has the highest CO_2 concentration because most of the cold fresh inlet air dwells near the bottom of the IVFS due to the buoyancy effect. In contrast, tray 3 has the lowest CO_2 concentration because the fresh inlet air has the highest flow resistance to reach tray 3

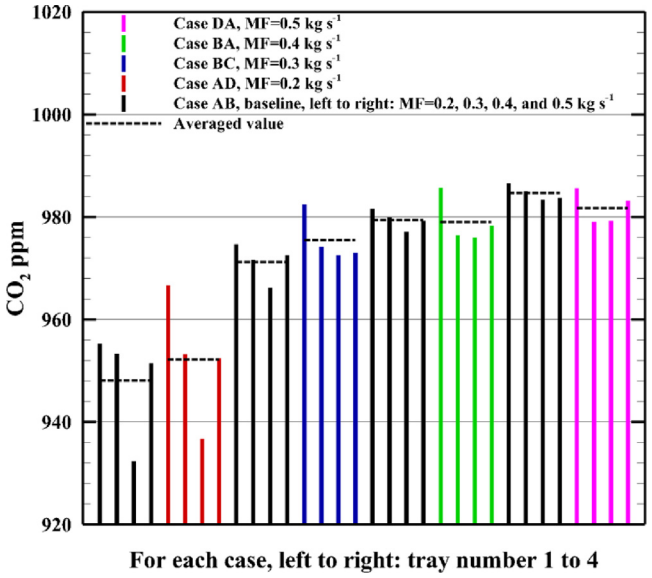

Fig. 10. Comparison of the average CO_2 concentration (ppm) over each tray between the best *OU* cases and the baseline case (AB) at each inlet mass flow rate condition.

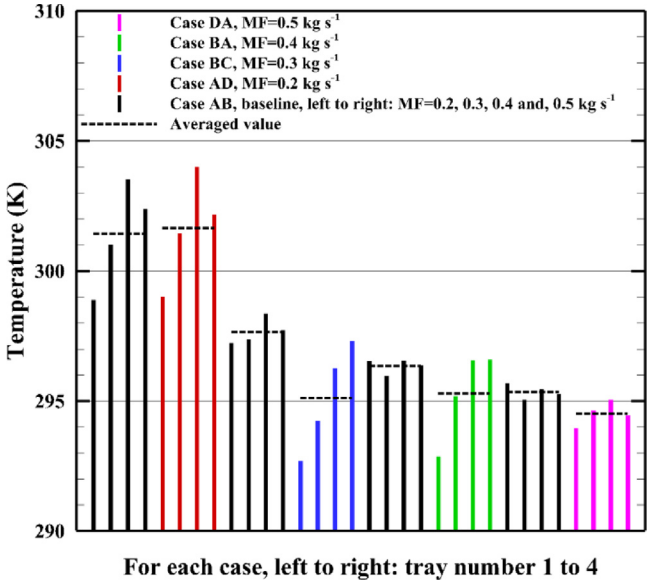

Fig. 11. Comparison of the average temperature over each tray between the best *OU* cases and the baseline case (AB) at each inlet mass flow rate condition.

due to the combination of sharp turns and buoyancy effect. This is particularly true at low inlet flow rates and when the inlet is located on the top, which lead to low flow circulation as cold inlet air flows downward directly. As a result, BC, BA, and DA at 0.3, 0.4, and 0.5 kg s^{-1}, respectively, have relatively high CO_2 concentrations. Even though the baseline case AB at 0.5 kg s^{-1} has the highest CO_2 concentration, its *OU* is too low to be considered a good design.

Temperature is also a critical parameter to control and monitor because it directly affects both relative humidity (*RH*) and plant growth [51]. The temperature distribution in the system depends on the inlet/exit location, inlet mass flow rate, and amount of heat. Since the inlet temperature and heat flux conditions are fixed, the exit temperature increases with decreasing inlet mass flow rate. Fig. 11 shows a comparison of the average temperatures of the higher *OU* cases and the baseline case AB at different inlet mass

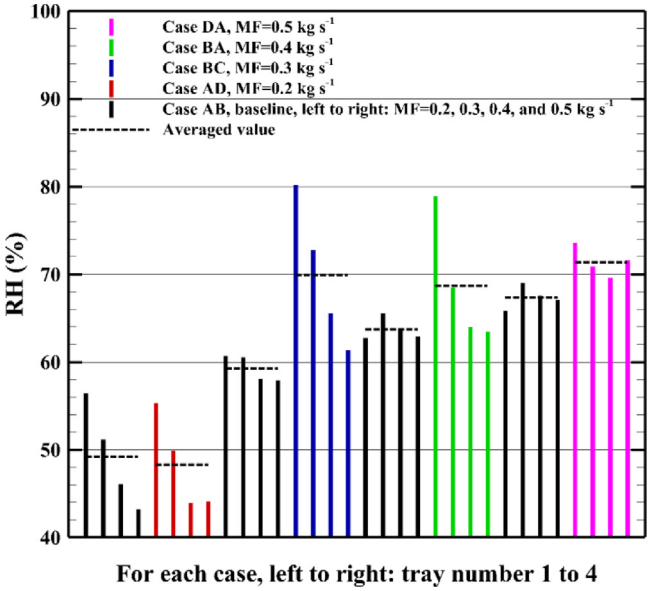

Fig. 12. Comparison of the average *RH* over each tray between the best *OU* cases and the baseline case (AB) at each inlet mass flow rate condition.

flow rates. Three phenomena can be observed from the baseline case AB results at different inlet mass flow rates: (1) the flow above tray 4 always has a lower temperature than that above tray 3 since it is closest to the inlet region; (2) at low inlet mass flow rate (< 0.3 kg s^{-1}), the flow above tray 3 has the highest temperature due to buoyancy effect; and (3) at high inlet mass flow rate (> 0.3 kg s^{-1}), the flow above tray 1 has the highest temperature because it is located closest to the exit.

The temperature distribution for case AD is very similar to that of the baseline case due to similar inlet/exit location orientations so that buoyancy is the dominant effect at low inlet mass flow rate (0.2 kg s^{-1}). On the other hand, cases BC, BA, and DA have different temperature distributions than the baseline because the inlet and exit are located near the bottom and the top, respectively. Therefore, the temperature of tray 1 is much closer to the inlet temperature (291.15 K) and the temperature increases with height except at high mass flow rate (> 0.4 kg s^{-1}) where the temperature above tray 4 can be lower than that above tray 3. This is due to strong helical flow mixing inside the room at high inlet mass flow rate, which also explains that the temperature uniformity increases with increasing inlet mass flow rate. Previous studies show that the optimal germination temperature is between 294 K and 297 K [52]. As can be observed from Fig. 11, cases BC, BA, and DA at 0.3, 0.4, and 0.5 kg s^{-1}, respectively, exhibit the desirable temperature range and distribution for lettuce growth. Nevertheless, compared to the baseline at each mass flow rate, case BC at an inlet mass flow rate of 0.3 kg s^{-1} exhibits the most significant average temperature reduction (2.54 K). Furthermore, the average temperature of case BC at 0.3 kg s^{-1} is lower than that of the baseline case at 0.5 kg s^{-1}, which demonstrates the design effectiveness of case BC.

Relative humidity (*RH*) represents the water vapor partial pressure in the IVFS, which has a strong effect on crop growth. It is reported that the ideal *RH* for lettuce and leafy greens should be between 50–70% [52]. High *RH* can cause pathogen issues, like mildew and botrytis, and low *RH* can induce an outer leaf edge burn due to dryness [51,52]. Therefore, the inlet *RH* is set to be 85% in this IVFS design. The comparison of *RH* for each tray between the highest *OU* and the baseline cases at different inlet mass flow rates is shown in Fig. 12. It can be observed from the baseline case that *RH* increases with increasing inlet mass flow rate due to

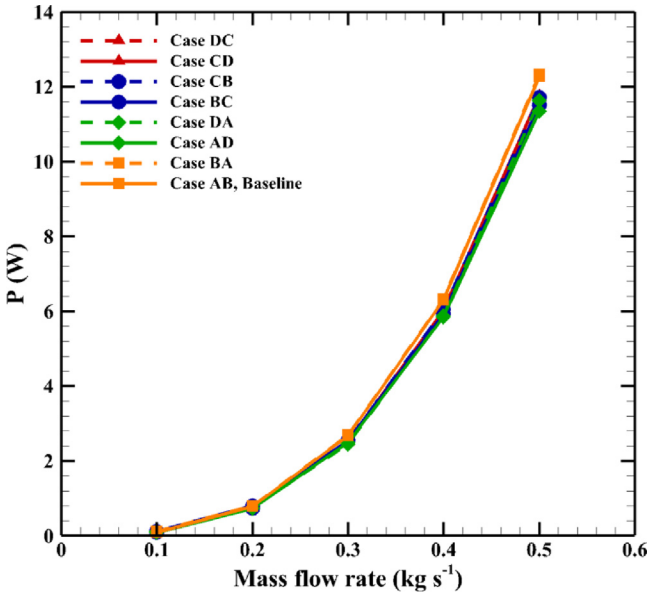

Fig. 13. Comparison of the power required to operate the flow circulation system between the best *OU* cases and the baseline case (AB) as a function of mass flow rate.

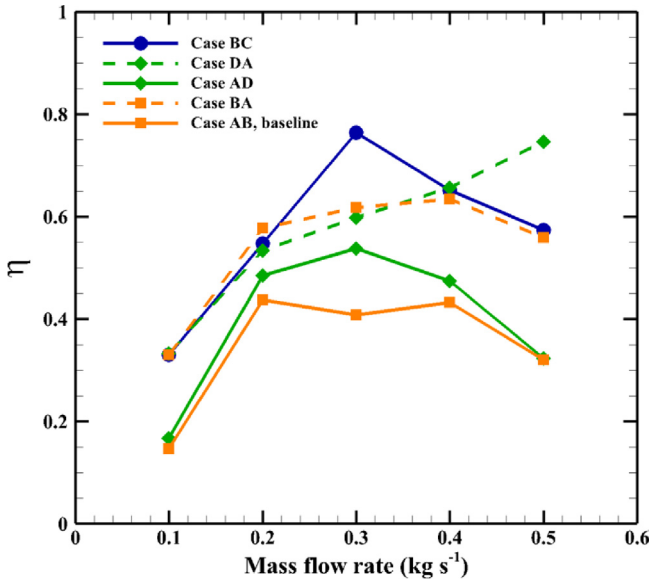

Fig. 14. Comparison of the overall efficiency between the best *OU* cases and the baseline case (AB) at each inlet mass flow rate condition.

the increase of water supply and decreasing room temperature. *RH* can be calculated from the ratio of the partial pressure of water vapor to the saturation vapor pressure at a given temperature. Therefore, *RH* can be increased by either increasing water partial pressure (molar ratio) or decreasing temperature. In our study, temperature is the dominant parameter because the gas species composition in the system does not vary significantly. Therefore, the trend of *RH* distribution agrees with that of the temperature distribution in Fig. 11. The only exception exists for the baseline case AB when the inlet mass flow rate is the smallest (0.2 kg s^{-1}). Under such conditions, tray 3 has higher temperature and *RH* than tray 4. To explain this behavior, the results from the CO_2 distribution analysis need to be considered. At the lowest inlet flow rate, the flow has lowest circulation and tray 3 is near the end of the fresh inlet flow stream. Therefore, tray 3 has the lowest CO_2 and highest H_2O concentrations due to photosynthesis as shown in Figs. 10 and 12. Overall, the average *RH* distributions for cases BC and BA fall within the optimal range.

6.3. Power requirement and the overall design efficiency

According to Eq. (8), the power required can be calculated as the product of volume flow rate and pressure drop between the inlet and exit. Even though the inlet/exit locations can change the overall system pressure drop slightly, mass flow rate has a dominating effect on the required power, as shown in Fig. 13. It can be observed that cases AB and BA incur the most pressure drop, which is more obvious at high flow rates. As discussed earlier, placing the inlet and exit on the same wall located at the short side disrupts the helical flow formation, which is known to benefit flow circulation. Under this condition (AB or BA), additional vertices, which is the main source of the increased pressure drop, are observed near the exit region from the flow streamlines. To minimize energy consumption, the inlet/exit location should be placed on opposite walls and the IVFS system should operate at the minimum flow rate that meets other requirements, such as temperature, *RH*, CO_2 concentration, and flow velocity above the exchange region.

Since there are multiple variables that can affect the overall design of the inlet/exit location and mass flow rate, an overall efficiency factor is introduced in Eq. (9) to holistically assess the uniformity of all monitored parameters. Fig. 14 shows the final comparison of the overall design efficiency between the four best *OU* cases and the baseline case. It can be observed that *OU* has a dominating effect on the overall efficiency since the trends show some resemblance to the overall efficiency. In terms of overall efficiency and power consumption, case BC operating at 0.3 kg s^{-1} is the optimal design for this IVFS.

7. Conclusion

In this work, a computational fluid dynamics model is developed to simulate the heat transfer and fluid flow in an indoor vertical farming system with photosynthesis. Eight cases of various inlet/exit location are studied under turbulent regime to evaluate flow velocity, temperature, relative humidity, CO_2 concentration and their distributions over each cultivation tray. Depending on the flow inlet/exit location, the objective uniformity varies between 39.6~91.7% when the mass flow rates ranges from 0.1~0.5 kg s^{-1}. The following two flow stream phenomena are observed to enhance the objective uniformity: 1) placing the flow inlet/exit location on opposite walls with inlet on the short side and exit on the long side to induce spiral flow for effective mixing; and 2) locating the flow inlet at the bottom and exit at the top to take advantage of the gravity-assisted buoyancy effect. However, higher objective uniformity does not necessarily lead to a more favorable species distribution. It was found that the lower tray has higher CO_2 concentration due to buoyancy effects. Further, in our eight studied cases, the tray near the middle height (tray 3) has the lowest CO_2 and highest H_2O concentrations due to less effective circulation. This trend is found to be more prominent when the mass flow rate is low. In addition, the case with inlet at the bottom of the short side and exit at the top of the long side running at 0.3 kg s^{-1} shows the desired lower average temperature compared to other inlet/exit locations operating at 0.4 or 0.5 kg s^{-1}. Accordingly, the reduced flow rate of 0.3 kg s^{-1} enables significant reduction in energy consumption. In conclusion, the newly-developed computational fluid dynamics model successfully demonstrates its capability to simulate heat transfer, fluid flow, and photosynthesis in an indoor vertical farming system. The simulation framework provides

a powerful tool to evaluate various design options and provide design guidance of indoor farming system.

Declaration of Competing Interest

The authors declare that they have no known competing financial interests or personal relationships that could have appeared to influence the work reported in this paper.

CRediT authorship contribution statement

Benyamin Naranjani: Data curation, Formal analysis, Methodology, Writing – original draft. **Zabihollah Najafianashrafi:** Data curation, Formal analysis, Writing – original draft. **Christopher Pascual:** Methodology, Writing – review & editing. **Ireneo Agulto:** Methodology, Writing – review & editing. **Po-Ya Abel Chuang:** Conceptualization, Methodology, Supervision, Funding acquisition, Writing – review & editing.

Acknowledgments

This study is supported by IVFS Programme (IIID 2017-18) from Commission on Higher Education - Philippine California Advanced Research Institutes (CHED-PCARI) of the Republic of the Philippines.

References

[1] B. Pandey, K.C. Seto, Urbanization and agricultural land loss in India: comparing satellite estimates with census data, J. Environ. Manag. 148 (2015) 53–66.
[2] R.E. Namara, M.A. Hanjra, G.E. Castillo, H.M. Ravnborg, L. Smith, B. Van Koppen, Agricultural water management and poverty linkages, Agric. Water Manag. 97 (4) (2010) 520–527.
[3] S. Piao, P. Ciais, Y. Huang, Z. Shen, S. Peng, J. Li, L. Zhou, H. Liu, Y. Ma, Y. Ding, The impacts of climate change on water resources and agriculture in China, Nature 467 (7311) (2010) 43–51.
[4] R. Dirzo, P.H. Raven, Global state of biodiversity and loss, Annu. Rev. Environ. Resour. 28 (1) (2003) 137–167.
[5] H.C.J. Godfray, J.R. Beddington, I.R. Crute, L. Haddad, D. Lawrence, J.F. Muir, J. Pretty, S. Robinson, S.M. Thomas, C. Toulmin, Food security: the challenge of feeding 9 billion people, Science 327 (5967) (2010) 812–818.
[6] T. Kozai, G. Niu, M. Takagaki, Plant factory: An Indoor Vertical Farming System for Efficient Quality Food Production, Academic press, 2019.
[7] E.F. Lambin, P. Meyfroidt, Global land use change, economic globalization, and the looming land scarcity, Proc. Natl. Acad. Sci. 108 (9) (2011) 3465–3472.
[8] Y. Shao, J. Li, Z. Zhou, Z. Hu, F. Zhang, Y. Cui, H. Chen, The effects of vertical farming on indoor carbon dioxide concentration and fresh air energy consumption in office buildings, Build. Environ. 195 (2021) 107766.
[9] T. Kozai, C. Chun, K. Ohyama, Closed systems with lamps for commercial production of transplants using minimal resources, in: Proceedings of the XXVI International Horticultural Congress: Nursery Crops; Development, Evaluation, Production and Use 630, 2002, pp. 239–254.
[10] T. Horibe, S. Imai, T. Matsuoka, Effects of light wavelength on daughter cladode growth and quality in edible cactus Nopalea cochenillifera cultured in a plant factory with artificial light, J. Hortic. Res. 26 (2) (2018).
[11] X. Deng, Y. Dou, D. Hu, Robust closed-loop control of vegetable production in plant factory, Comput. Electron. Agric. 155 (2018) 244–250.
[12] Y. Kurashina, T. Yamashita, S. Kurabayashi, K. Takemura, K. Ando, Growth control of leaf lettuce with exposure to underwater ultrasound and dissolved oxygen supersaturation, Ultrason. Sonochem. 51 (2019) 292–297.
[13] M.R. Talukder, M. Asaduzzaman, H. Tanaka, T. Asao, Application of alternating current electro-degradation improves retarded growth and quality in lettuce under autotoxicity in successive cultivation, Sci. Hortic. 252 (2019) 324–331.
[14] T. Kozai, G. Niu, in: Plant Factory As a Resource-Efficient Closed Plant Production system, in: Plant Factory, Elsevier, 2016, pp. 69–90.
[15] K. Yabuki, Photosynthetic Rate and Dynamic Environment, Springer Science & Business Media, 2004.
[16] J.G. Lee, C.S. Choi, Y.A. Jang, S.W. Jang, S.G. Lee, Y.C. Um, Effects of air temperature and air flow rate control on the tipburn occurrence of leaf lettuce in a closed-type plant factory system, Hortic. Environ. Biotechnol. 54 (4) (2013) 303–310.
[17] T. Kuronuma, Y. Watanabe, M. Ando, H. Watanabe, Tipburn severity and calcium distribution in lisianthus (Eustoma Grandiflorum (Raf.) Shinn.) cultivars under different relative air humidity conditions, Agronomy 8 (10) (2018) 218.
[18] P. Vanhassel, P. Bleyaert, J. Van Lommel, I. Vandevelde, S. Crappé, N. Van Hese, J. Hanssens, K. Steppe, M.C. Van Labeke, Rise of nightly air humidity as a measure for tipburn prevention in hydroponic cultivation of butterhead lettuce, in: Proceedings of the XXIX International Horticultural Congress on Horticulture: Sustaining Lives, Livelihoods and Landscapes (IHC2014): 1107, 2014, pp. 195–202.
[19] M.-.S. Baek, S.-.Y. Kwon, J.-.H. Lim, Improvement of uniformity in cultivation environment and crop growth rate by hybrid control of air flow devices, J. Cent. South Univ. 22 (12) (2015) 4702–4708.
[20] Y. Zhang, M. Kacira, in: Air Distribution and Its Uniformity, Smart Plant Factory, Springer, 2018, pp. 153–166.
[21] N. Markatos, M. Malin, G. Cox, Mathematical modelling of buoyancy-induced smoke flow in enclosures, Int. J. Heat Mass Transf. 25 (1) (1982) 63–75.
[22] G. Stavrakakis, M. Koukou, M.G. Vrachopoulos, N. Markatos, Natural cross-ventilation in buildings: building-scale experiments, numerical simulation and thermal comfort evaluation, Energy Build. 40 (9) (2008) 1666–1681.
[23] K. Papakonstantinou, C.T. Kiranoudis, N.C. Markatos, Computational analysis of thermal comfort: the case of the archaeological museum of Athens, Appl. Math. Model. 24 (7) (2000) 477–494.
[24] W.L. Li, J.H. Wang, Y.C. Lu, L. Shao, G.W. Chu, Y. Xiang, CFD analysis of CO2 absorption in a microporous tube-in-tube microchannel reactor with a novel gas-liquid mass transfer model, Int. J. Heat Mass Transf. 150 (2020) 119389.
[25] R. Yuan, N. Dutta, S. Sivasankaran, W. Jansen, K. Ebrahimi, Heat retention analysis with thermal encapsulation of powertrain under natural soak environment, Int. J. Heat Mass Transf. 147 (2020) 118940.
[26] J. Serrano-Arellano, M. Gijón-Rivera, J. Riesco-Ávila, J. Xamán, G. Álvarez, Numerical investigation of transient heat and mass transfer by natural convection in a ventilated cavity: outlet air gap located close to heat source, Int. J. Heat Mass Transf. 76 (2014) 268–278.
[27] N. Gupta, A. Nayak, S. Malik, Conjugate heat and species transport in an air filled ventilated enclosure with a thermo-contaminated block, Int. J. Heat Mass Transf. 117 (2018) 388–411.
[28] D. Liu, F.Y. Zhao, H. Yang, J. Chen, C. Ye, Probability adjoint identification of airborne pollutant sources depending on one sensor in a ventilated enclosure with conjugate heat and species transports, Int. J. Heat Mass Transf. 102 (2016) 919–933.
[29] M. Santos, D. Oliveira, J. Campos, T. Mayor, Numerical analysis of the flow and heat transfer in cylindrical clothing microclimates–Influence of the microclimate thickness ratio, Int. J. Heat Mass Transf. 117 (2018) 71–79.
[30] Y. Zhang, M. Kacira, L. An, A CFD study on improving air flow uniformity in indoor plant factory system, Biosyst. Eng. 147 (2016) 193–205.
[31] D. Karadimou, N. Markatos, Modelling of two-phase, transient airflow and particles distribution in the indoor environment by large eddy simulation, J. Turbul. 17 (2) (2016) 216–236.
[32] M.S. Baek, S.Y. Kwon, J.H. Lim, Improvement of the crop growth rate in plant factory by promoting air flow inside the cultivation, Int. J. Smart Home 10 (2) (2016) 63–74.
[33] A. Niam, T. Muharam, S. Widodo, M. Solahudin, L. Sucahyo, CFD simulation approach in determining air conditioners position in the mini plant factory for shallot seed production, in: Proceedings of the AIP Conference Proceedings, AIP Publishing LLC, 2019.
[34] M.A. El-Sharkawy, Overview: early history of crop growth and photosynthesis modeling, BioSystems 103 (2) (2011) 205–211.
[35] T. Boulard, J.C. Roy, J.B. Pouillard, H. Fatnassi, A. Grisey, Modelling of micrometeorology, canopy transpiration and photosynthesis in a closed greenhouse using computational fluid dynamics, Biosyst. Eng. 158 (2017) 110–133.
[36] B.O. Jin, C.H. Kim, M.H. Kim, G.Y. Baek, E.G. Choi, B.E. Moon, S.Y. Lee, H.T. Kim, Estimate of CO2 consumption in lettuce according to the leaf area, IFAC Proc. Vol. 46 (4) (2013) 71–74.
[37] O. Adeyemi, I. Grove, S. Peets, Y. Domun, T. Norton, Dynamic modelling of lettuce transpiration for water status monitoring, Comput. Electron. Agric. 155 (2018) 50–57.
[38] P. Bournet, S.O. Khaoua, T. Boulard, Numerical prediction of the effect of vent arrangements on the ventilation and energy transfer in a multi-span glasshouse using a bi-band radiation model, Biosyst. Eng. 98 (2) (2007) 224–234.
[39] K. Kim, J.Y. Yoon, H.J. Kwon, J.H. Han, J.E. Son, S.W. Nam, G.A. Giacomelli, I.B. Lee, 3-D CFD analysis of relative humidity distribution in greenhouse with a fog cooling system and refrigerative dehumidifiers, Biosyst. Eng. 100 (2) (2008) 245–255.
[40] A. Mistriotis, G. Bot, P. Picuno, G. Scarascia-Mugnozza, Analysis of the efficiency of greenhouse ventilation using computational fluid dynamics, Agric. For. Meteorol. 85 (3–4) (1997) 217–228.
[41] J.P. Van Doormaal, G.D. Raithby, Enhancements of the SIMPLE method for predicting incompressible fluid flows, Numer. Heat Transf. 7 (2) (1984) 147–163.
[42] T. Shibuya, J. Tsuruyama, Y. Kitaya, M. Kiyota, Enhancement of photosynthesis and growth of tomato seedlings by forced ventilation within the canopy, Sci. Hortic. 109 (3) (2006) 218–222.
[43] S. Nakagawa, M. Senda, A. Hiraide, S. Kikkawa, Heat transfer characteristics in a channel flow with a rectangular cylinder, JSME Int. J. Ser. B Fluids Therm. Eng. 42 (2) (1999) 188–196.
[44] D.A. Lyn, S. Einav, W. Rodi, J.H. Park, A laser-doppler velocimetry study of ensemble-averaged characteristics of the turbulent near wake of a square cylinder, J. Fluid Mech. 304 (1995) 285–319.
[45] R. Franke, W. Rodi, in: Calculation of Vortex Shedding Past a Square Cylinder With Various Turbulence models, in: Turbulent shear Flows 8, Springer, 1993, pp. 189–204.

[46] D. Durao, M. Heitor, J. Pereira, Measurements of turbulent and periodic flows around a square cross-section cylinder, Exp. Fluids 6 (5) (1988) 298–304.
[47] T. Bartzanas, T. Boulard, C. Kittas, Effect of vent arrangement on windward ventilation of a tunnel greenhouse, Biosyst. Eng. 88 (4) (2004) 479–490.
[48] C. Wang, Y. Zhang, D. Zhang, Z. Lan, W. Tian, G. Su, S. Qiu, Numerical study of oxygen transport characteristics in lead-bismuth eutectic for gas-phase oxygen control, Nucl. Eng. Technol. 53 (7) (2021) 2221–2228.
[49] A. Spille-Kohoff, E. Preuß, K. Böttcher, Numerical solution of multi-component species transport in gases at any total number of components, Int. J. Heat Mass Transf. 55 (19–20) (2012) 5373–5377.
[50] Y. Zheng, F. Li, L. Hao, A.A. Shedayi, L. Guo, C. Ma, B. Huang, M. Xu, The optimal CO 2 concentrations for the growth of three perennial grass species, BMC Plant Biol. 18 (1) (2018) 1–12.
[51] J. Ben-Asher, A.G. y Garcia, I. Flitcroft, G. Hoogenboom, Effect of atmospheric water vapor on photosynthesis, transpiration and canopy conductance: a case study in corn, Plant Soil Environ. 59 (12) (2013) 549–555.
[52] M. Brechner, A. Both, C. Staff, Hydroponic lettuce handbook, Cornell Controll. Environ. Agric. 834 (1996) 504–509.